Lack of R-Ras Leads to Increased Vascular Permeability in Ischemic Retinopathy

Maria Vähätupa,[1,2] Stuart Prince,[2] Suvi Vataja,[1] Teija Mertimo,[1] Marko Kataja,[3] Kati Kinnunen,[4] Varpu Marjomäki,[5] Hannu Uusitalo,[1,3] Masanobu Komatsu,[6] Tero A.H. Järvinen,[2,7] and Hannele Uusitalo-Järvinen[1,3]

[1]Department of Ophthalmology, University of Tampere, Tampere, Finland
[2]Department of Anatomy, University of Tampere, Tampere, Finland
[3]Eye Centre, Tampere University Hospital, Tampere, Finland
[4]Department of Ophthalmology, Kuopio University Hospital, Kuopio, Finland
[5]Department of Biological and Environmental Science/Nanoscience Center, University of Jyväskylä, Jyväskylä, Finland
[6]Sanford Burnham Prebys Medical Discovery Institute at Lake Nona, Orlando, Florida, United States
[7]Department of Musculoskeletal Disorders, Tampere University Hospital, Tampere, Finland

Correspondence: Hannele Uusitalo-Järvinen, Department of Ophthalmology, School of Medicine, 33014 University of Tampere, Finland; llhauus@uta.fi.

Submitted: January 25, 2016
Accepted: July 14, 2016

Citation: Vähätupa M, Prince S, Vataja S, et al. Lack of R-Ras leads to increased vascular permeability in ischemic retinopathy. *Invest Ophthalmol Vis Sci*. 2016;57:4898–4909. DOI:10.1167/iovs.16-19212

Purpose. The role of R-Ras in retinal angiogenesis and vascular permeability was evaluated in an oxygen-induced retinopathy (OIR) model using R-Ras knockout (KO) mice and in human diabetic neovascular membranes.

Methods. Mice deficient for R-Ras and their wild-type (WT) littermates were subjected to 75% oxygen from postnatal day 7 (P7) to P12 and then returned to room air. At P17 retinal vascularization was examined from whole mounts, and retinal vascular permeability was studied using Miles assay. Real-time RT-PCR, Western blotting, and immunohistochemistry were used to assess the expression of R-Ras in retina during development or in the OIR model. The degree of pericyte coverage and vascular endothelial (VE)-cadherin expression on WT and R-Ras KO retinal blood vessels was quantified using confocal microscopy. The correlation of R-Ras with vascular endothelial growth factor receptor 2 (VEGFR2) and human serum albumin on human proliferative diabetic retinopathy membranes was assessed using immunohistochemistry.

Results. In retina, R-Ras expression was mostly restricted to the vasculature. Retinal vessels in the R-Ras KO mice were significantly more permeable than WT controls in the OIR model. A significant reduction in the direct physical contact between pericytes and blood vessel endothelium as well as reduced VE-cadherin immunostaining was found in R-Ras–deficient mice. In human proliferative diabetic retinopathy neovascular membranes, R-Ras expression negatively correlated with increased vascular leakage and expression of VEGFR2, a marker of blood vessel immaturity.

Conclusions. Our results suggest that R-Ras has a role in controlling retinal vessel maturation and stabilization in ischemic retinopathy and provides a potential target for pharmacologic manipulation to treat diabetic retinopathy.

Keywords: retina, diabetic retinopathy, neovascularization, retinal ischemia

Diabetic macular edema (DME) and proliferative diabetic retinopathy (PDR) are the two forms of diabetic retinopathy causing blindness. Vascular endothelial growth factor (VEGF) plays a crucial role in these diseases by causing vascular leakage and pathologic neovascularization.[1–3] Anti-VEGF drugs are regarded as the mainstay of treatment for patients affected by DME. However, VEGF inhibition fails to provide sufficient efficacy in all DME cases; only half of patients attain significant improvement in visual acuity.[4] Anti-VEGF therapy is also accompanied by rare, but severe, ocular and systemic side effects. In PDR, anti-VEGF may be associated with development of tractional retinal detachment[5,6] Furthermore, intravitreally administered anti-VEGF agents may cause sustained systemic VEGF inhibition[7,8] This is why they are relatively contraindicated in pregnant women[9] and patients with cardiovascular insufficiency.[10,11] Thus, alternative therapies are needed for more effective and safer treatment of diabetic retinopathy.[12,13]

R-Ras is a small GTPase of the Ras family of oncogenes.[14] Despite the close structural similarity to other members of the Ras family, the function of R-Ras is distinct from other Ras proteins.[15] Whereas all other members of the Ras family may cause malignant transformation, R-Ras has very little or no transforming activity.[16] Furthermore, the opposing functions of R-Ras and H-Ras extend to cell–extracellular matrix (ECM) adhesion,[17] cell differentiation,[18] and signaling.[19] These opposing functions have led to the suggestion that the balance between R-Ras and other Ras members acts as a switch that controls proliferation and invasion versus quiescence in cells.[15,20,21]

Recently, active Ras signaling has been implicated as a key driver of pathologic angiogenesis in neovascular diseases of the

retina.[22] Conversely, exactly the opposite role has recently been shown for R-Ras in the regulation of angiogenesis.[20] R-Ras function has been shown to be essential for the establishment of mature and functional blood vessels in tumors by stabilization of immature, leaky vessels, enhancing perfusion and ultimately reducing plasma leakage.[15,21] Based on these functions, R-Ras has been classified as an antiangiogenic molecule. However, R-Ras is functionally different from classic antiangiogenic agents as it does not induce endothelial cell apoptosis as do other antiangiogenic molecules, but actually promotes endothelial cell survival.[20] Thus, R-Ras could provide a potential agonistic therapeutic target for treatment of a variety of retinal diseases associated with ischemia, neovascularization, and vascular leakage. In the present study, the role of R-Ras in the retina was studied by analyzing expression of R-Ras in the retina and by analyzing the effect of R-Ras deficiency on the structural and functional integrity of retinal vasculature during development and ischemic retinopathy using an oxygen-induced retinopathy model (OIR). To address the role of R-Ras in PDR, association of its expression with vascular immaturity and leakiness was examined in human retinal neovascular membranes.

Methods

Mice

For the experiments, wild-type (WT) C57BL/6 mice from Harlan Sprague Dawley (Indianapolis, IN, USA) and homozygous R-Ras knockout (KO) mice were used. R-Ras KO mice with an insertion deleting R-Ras expression between exons 4 and 5 of *Rras* on chromosome 7 (R-Ras KO mice) have been described previously.[20] Before any experiments, R-Ras heterozygous mice were backcrossed eight times with the C57BL/6 strain to obtain homozygous KO and WT mice in the same genetic background. The mice were bred, and the genotype was determined by PCR. Mice were fed with standard laboratory pellets and water ad libitum. All animal experiments were performed according to the ARVO Statement for the Use of Animals in Ophthalmic and Vision Research in accordance with protocols approved by the National Animal Ethics Committee of Finland.

Oxygen-Induced Retinopathy Model

The experiments on the OIR model were carried out as described in detail previously.[23,24] Briefly, neonatal mice at postnatal day 7 (P7) were exposed to 75% oxygen for 5 days. At P12, they were returned to normal room air.[23] Animals were euthanized at P12 to assess the degree of vascular regression and at P17 to determine the rate of retinal revascularization and preretinal neovascularization. As postnatal weight gain has been shown to affect outcome in the OIR model,[25] only the pups weighing between 6.3 and 7.5 g at P17 were included in the study.

Immunohistochemistry (IHC) and Isolectin GS-IB_4 Staining

For the analysis of retinal vasculature, eyes were enucleated, fixed with 4% paraformaldehyde (PFA), and retinas dissected. Flat-mount retinas were blocked in 20% normal goat and 20% fetal bovine serums for 2 hours, incubated overnight Isolectin (Isolectin GS-IB_4, 1:200; Invitrogen, Carlsbad, CA, USA) and with anti-NG2 chondroitin sulfate proteoglycan antibody (1:80; Millipore, Billerica, MA), followed by Alexa Fluor-conjugated secondary antibody. Retinas were imaged via confocal microscope (LSM 700; Carl Zeiss, Oberkochen, Germany) and the rate of angiogenesis was determined during development (P0–P6) and in the OIR model as previously described.[24] Briefly, retinas were imaged using confocal microscopy (Carl Zeiss LSM 700) with 5× objective. By focusing just above the inner limiting membrane of the retina, the preretinal neovascular tufts were readily distinguished from the underlying superficial vascular plexus. Areas of vascular obliteration and pathologic neovascularization (meaning neovascular tufts) were quantified from these images using image editing software (Adobe Photoshop CS3; Adobe Systems, Inc., San Jose, CA, USA). The rate of developmental angiogenesis at P0 to P6 was determined by measuring the length of vasculature from the optic nerve to the tips of the blood vessels. Four measurements per retina were taken and an average was calculated.

For immunohistochemistry, the eyes were fixed with 4% PFA and embedded in paraffin or immediately frozen in ornithine carbamoyltransferase embedding compound in isopentane cooled with liquid nitrogen and later fixed with acetone. The IHC was carried out on 4- to 6-μm-thick tissue sections using the following primary antibodies: rabbit anti–R-Ras (1:50) and rabbit anti-VEGFR2 (1:100; both Cell Signaling Technology, Danvers, MA, USA), rabbit anti–R-Ras (1:750) and mouse anti-VEGFR2 (1:200, clone sc.6251; both Santa Cruz Biotechnology, Dallas, TX, USA), rat anti-mouse CD31 (1:50; BD Pharmingen, San Diego, CA, USA), guinea pig anti-NG2 antibody (1:100, gift from William Stallcup),[26] rabbit anti-Syndecan (1:500) and rabbit anti-human vascular endothelial (VE)-cadherin (1:500; both from Abcam, Cambridge, UK), and rabbit anti-human serum albumin (1:100; Lifespan Biosciences, Seattle, WA, USA), followed by horseradish peroxidase (HRP) or fluorescein-conjugated secondary antibodies. Hematoxylin staining was used as a counterstain. Samples were mounted with Vectashield mounting medium with 4′,6-diamidino-2-phenylindole (Vector Laboratories) and analyzed via confocal microscope. Each staining experiment included sections stained without primary antibody as negative controls. Percentage of R-Ras positive cells in preretinal neovessels were quantified manually by using the count tool in Adobe Photoshop (Adobe Systems, Inc.) ($n = 6$ mice, 4–6 sections/retina).

Quantification of Pericyte Coverage and VE-Cadherin Colocalization With CD31

Pericyte coverage of the blood vessels was quantified from WT and R-Ras KO P17 OIR model whole-mount retinas. Samples were imaged using confocal microscopy (Carl Zeiss LSM 700) with a 63× objective lens, and 3D pictures were made from Z-stacks. Pictures selected for the analysis were randomly taken from Isolectin IB_4 and NG2-stained flat-mounts from the most superficial vascular plexus at the tips of the blood vessels next to avascular area. This is a region of retina where the blood vessels are growing toward the optic nerve. Direct contact between pericytes (NG2) and endothelial cells (Isolectin B_4) were quantified by colocalization analysis with BioImageXD (provided in the public domain at http://www.bioimagexd.org).[27] The percentage of EC area colocalized with pericyte area was quantified in each image, and the result expressed as a mean of two different images for each retina. The intensity of VE-cadherin staining and colocalization of VE-cadherin and CD31 was quantified from frozen sections using BioImage XD.

Real-Time Quantitative PCR (qPCR)

Eyes were collected at P0, P4, P7, P12, P17, and P22 and placed immediately in cold RNA stabilization reagent (RNAlater; Sigma-Aldrich Corp., St. Louis, MO, USA) for the

Investigative Ophthalmology & Visual Science

duration of dissection of the retinas. RNA was extracted using RNA isolation kit (RNeasy Mini Kit; Qiagen, Hilden, Germany) following the manufacturer's instructions. The integrity of extracted RNA was verified on formaldehyde agarose gel. Reverse transcription of RNA was carried out using cDNA synthesis kit (Maxima First Strand cDNA Synthesis Kit; Thermo Fisher Scientific, Boston, MA, USA), according to the manufacturer's instructions. Real-time qPCR was done using the PCR dye (SYBR Green; Thermo Fisher Scientific) method according to the manufacturer's recommendations and performed in white 96-well plates (Multiply PCR plates; Sarstedt, Nümbrecht, Germany). The fluorescence signal was detected using a sequence detection system (ABI Prism 7000 Sequence Detection System 1.2; Applied Biosystems, Carlsbad, CA, USA). The following intron-spanning primers specific for exon 3 and 4 of *Rras* were used: 5′-ACAGGCA GAGTTTCAATGAG-3′ (forward), 5′-GTTCTCCAGATCTGCC TTG-3′ (reverse). *Ppia* was used as an endogenous control gene (5′-CACCGTGTTCTTCGACATC-3′ and 5′-ATTCTGTGA AAGGAGGAACC-3′), allowing the comparison of samples.[20] Two or three replicates were analyzed for each sample, and the results were expressed as a mean for each sample. Negative, no template (NTC) and no reverse transcriptase (no RT), controls were included in every qPCR analysis. A melting curve analysis was performed to check for unspecific PCR products (which didn't occur). Reaction efficiencies for both primer pairs were tested with standard curve analysis in different time points. Due to similar efficiencies for both primer pairs, the differences in gene expression levels were determined by the comparative Ct method (ΔΔCt method).[28]

Vascular Permeability Assay

Vascular permeability was quantified by Miles assay in retinas as described previously.[29] Briefly, the mice were injected with 2% Evans Blue ([EB], 150 μL/20g; Sigma-Aldrich Corp.) intraperitoneally, and the circulation time was 24 h for P16 or 1 hour for P17 injected mice. Phosphate-buffered saline–injected mice were used as a negative control. Animals were euthanized at P17, and blood was collected from the left ventricle. Retinas were dissected and weighed. Blood was centrifuged at 3,550*g* for 15 minutes, and plasma was diluted 1:100 and 1:1000 in N, N-dimethylformamide (Sigma-Aldrich Corp.). All samples were incubated in a shaker (100 rpm) in 200 μL N, N-dimethylformamide overnight at 78°C. Retinas were centrifuged at 17,000*g* for 45 minutes at 4°C, and the supernatants were collected. The EB absorbance of each sample was measured at 620 nm by spectrophotometer. EB concentration in the retina was proportioned and normalized by the weight of the retina and the amount of EB concentration in the plasma.[30]

Western Blotting

Retinas were lysed in 10 μL of cold RIPA buffer per 1 mg of tissue with added protease inhibitor (c*O*mplete; Roche, Basel, Switzerland) and phosphatase inhibitor (Halt; Thermo Fisher Scientific).

The tissues were homogenized using CK14 beads and a tissue homogenizer (Precellys; Bertin Technologies, Montigny le-Bretonneux, France). From each sample, 40 μg of protein was loaded per well of a 4-12% gradient gel (NuPAGE; Invitrogen, Carlsbad, CA, USA) and electroblotted on polyvinylidene fluoride membranes (Immun-Blo; Bio-Rad Laboratories, Hercules, California). For detection of specific proteins by immunoblotting, the following primary antibodies were used: rabbit anti–R-Ras (1:500; Cell Signaling Technology), goat anti-GAPDH (1:500: AbCam) and horse anti-mouse IgG (1:2000; Cell Signaling Technology). Primary antibodies were detected by HRP-coupled antibodies. Western blot images were captured via software (ImageQuant; GE Healthcare, Chalfont St. Giles, UK) and quantified by densitometry using Adobe Photoshop CS3 software, where GAPDH was used to normalize for protein loading. A calibrator control sample was included in every membrane to enable sample comparison between different membranes.

Retinal and Neovascular Samples From Human Patients

Preretinal neovascular membranes were obtained from eight type I diabetic patients who were undergoing pars plana vitrectomy for the treatment of PDR. All patients were Caucasians, and altogether there were five females and three males. At the time of pars plana, vitrectomy patients' mean age was 33 years (range, 27–56 years) and mean duration of diabetes was 24 years (range, 16–32 years). Normal human retinas were obtained from patients whose eyes were enucleated due to choroidal melanoma. The protocol for collecting human tissue samples was approved by the institutional review boards of the Pirkanmaa Hospital District and the Kuopio University Hospital. The study was conducted in accordance with the Declaration of Helsinki. All patients gave written informed consent. During vitrectomy, the fibrovascular membranes were isolated, grasped with vitreous forceps, and pulled out through a sclerotomy. The sample was immediately fixed with 4% formaldehyde for 3 h, transferred to 70% ethanol, embedded in paraffin, and processed for immunohistochemistry. The number of R-Ras–positive neovessels was calculated from CD31 and R-Ras–double-stained tissue sections, and correlation between R-Ras and VEGFR2 was quantified from R-Ras and VEGFR2 double-stained sections. Immunohistochemistry against human serum albumin (HSA) was done to quantify the amount of vascular leakage outside the neovessels. Quantification was done using IHC Profiler plugin in ImageJ software (http://imagej.nih.gov/ij/; provided in the public domain by National Institutes of Health, Bethesda, MD, USA). The area of positive staining for HSA was compared to the total analyzed area, and correlation analysis between HSA and percentage of R-Ras–positive neovessels was performed for each sample.

Statistical Analysis

Student's *t*-test was conducted for normally distributed data and nonparametric Mann-Whitney *U* test using statistical software (GraphPad Prism 6.01; GraphPad Software, San Diego, CA, USA, and IBM SPSS Statistics; IBM, Amonk, NY, USA) for nonnormally distributed data to test the statistical significance of the results. Spearman's rank correlation test was conducted to test correlation between two variables. *P* values less than 0.05 were considered statistically significant.

Results

R-Ras Expression Peaks During Retinal Developmental Angiogenesis But Does Not Influence the Rate of Developmental Angiogenesis

R-Ras KO mice are fertile and show no obvious morphologic abnormalities,[20,31] and their eyes appear normal upon histologic examination. To address the role of R-Ras on retinal angiogenesis in vivo, the expression profile of R-Ras in the

Investigative Ophthalmology & Visual Science

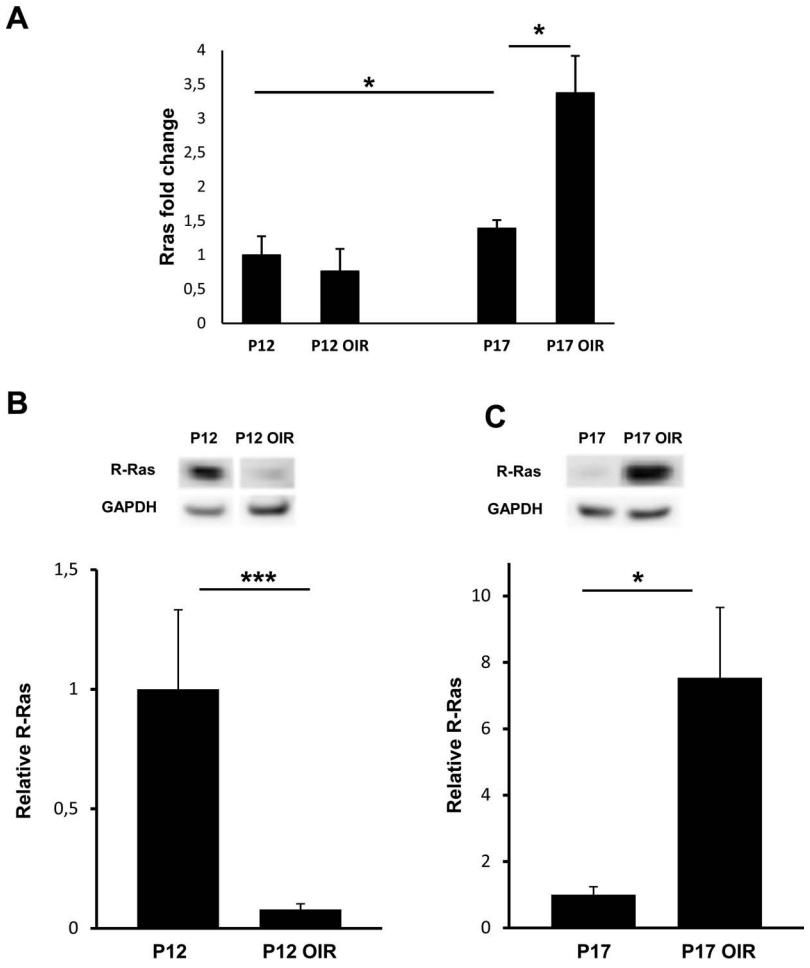

Figure 1. Hypoxia-driven R-Ras expression in the OIR model. Hypoxia-induced angiogenesis in retina was studied with the OIR model. Retinas were harvested immediately after the exposure to hyperoxia (P12) and after hypoxia-driven pathologic angiogenesis has reached its maximum at P17. Retinas from normal mice were harvested at corresponding time points. Retinas were subjected to either quantitative mRNA (real-time qPCR) analysis using SYBR Green method or protein (Western blotting) analysis. For immunoblotting, retinal protein supernatants were electrophoresed on gradient gels, standard Western blotting was carried out with R-Ras–specific antibody, and GAPDH detection was used as a loading control. (**A**) The graph represents fold changes ($2^{-\Delta\Delta Ct}$ method) in the *Rras* mRNA expression level relative to the *Rras* mRNA expression level of normal mice at P12. The level of *Rras* mRNA expression between normal and OIR model retinas is equal at P12, whereas at P17 hypoxia leads to 2.5-fold upregulation of *Rras* mRNA ($P = 0.016$, * nonparametric Mann-Whitney *U* test). *Error bars* represent the minimum and maximum of the fold change. (P12, P17 OIR: $n = 4$; P17, P12 OIR: $n = 5$.) (**B**, **C**) The level of R-Ras protein expression was quantified by densitometric analysis of immunoblotted protein. R-Ras protein level at P17 shows a 7.5-fold increase ($P = 0.016$) during hypoxia-induced angiogenesis. *Error bars* represent ± 95% confidence intervals. (P12: $n = 6$; P12 OIR: $n = 7$; P17: $n = 5$; P17: $n = 5$.) The results are analyzed with nonparametric Mann-Whitney *U* test. The samples presented above were run on the same gel. Representative samples were cropped and presented side-by-side.

developing mouse retina as well as the developmental rate of angiogenesis in WT and R-Ras KO mice were characterized.

To assess the temporal expression pattern of R-Ras during developmental retinal angiogenesis, qPCR and Western blot analysis were used. Quantitative PCR demonstrated that the *Rras* mRNA expression increased from P0 onward, peaked at P17, and started to decline from P17 until P22. Western blot analysis demonstrated a R-Ras protein expression profile similar to the mRNA profile: an increase in expression from P0 until P17 and a decline from P17 to P22 (Supplementary Fig. S1). The increase in *Rras* mRNA and protein levels from P0 to P17 correlates with the development of retinal vascular plexuses.[32] The R-Ras levels peaked at P17, when all three vascular plexuses are formed and vascular density peaks in the retina[33] (Supplementary Fig. S1). The findings are consistent with the notion that R-Ras appears in the blood vessels during their differentiation and is most strongly expressed in fully differentiated, quiescent blood vessels.[20] The reduction in *Rras* mRNA and protein expression levels from P17 to P22 can be explained by the remodeling of retinal vasculature (including vascular pruning), the outcome of which is decreased endothelial cell density at P28.[34] Consistent with this finding, the results show a similar decrease in the intensity of Isolectin IB_4 staining from P12 onward (Supplementary Fig. S2). No R-Ras protein or mRNA expression was detected in the retinas collected from R-Ras KO mice.

To explore whether the increase in R-Ras expression level seen during retinal development influences the rate of superficial vascular plexus formation (developmental angiogenesis), retinas from P0, P2, P4, and P6 WT and R-Ras KO mice were analyzed. In P0, P2, P4, and P6 neonatal mice, the diameter of retinal superficial vascular plexuses were similar both in R-Ras KO and WT mice, indicating that R-Ras expression is not necessary for in vivo angiogenesis during neonatal development (Supplementary Fig. S3). The lack of

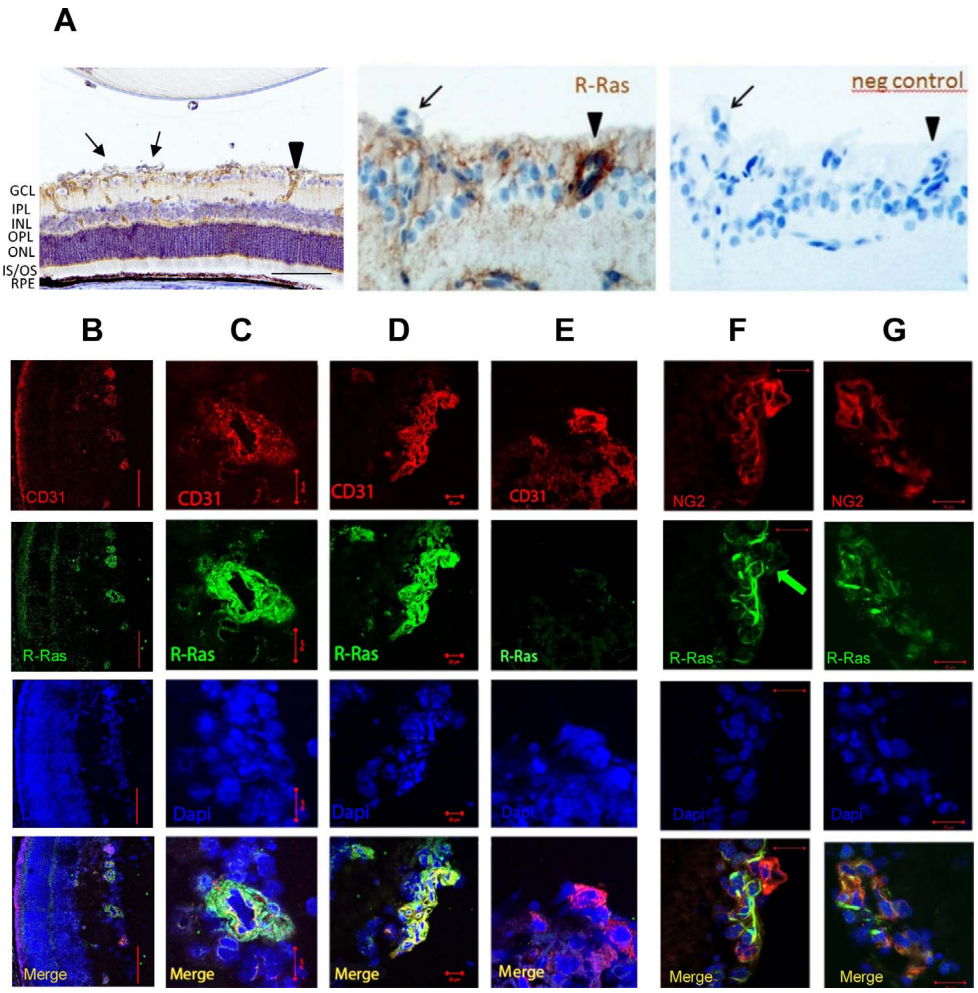

Figure 2. R-Ras is strongly, but selectively expressed in the endothelial cells and pericytes of blood vessels in retina. Oxygen-induced retinopathy was induced by exposing WT pups to 75% oxygen at P7 for 5 days and returning them to normal room air at P12. After 5 days in normoxia (at P17), the R-Ras expression was determined from the revascularized retinas by IHC and immunofluorescence (IF) using R-Ras–specific primary antibody. (**A**) Representative images of R-Ras expression in the OIR model. More than 30% of the preretinal blood vessels are negative for R-Ras (*arrow*), whereas blood vessels in retina are R-Ras positive (*arrowhead*). *Right*, negative control (no primary antibody). There is also faint R-Ras expression from other retinal cells, presumably from neural cells in the retina. GCL, ganglion cell layer; IPL, inner plexiform layer; INL, inner nuclear layer, OPL, outer plexiform layer; ONL, outer nuclear layer; IS/OS, photoreceptor inner/outer segments; RPE, retinal pigment epithelium. (**B–E**) Representative confocal images showing the colocalization of R-Ras (*green*) and CD31 (*red*) in the retina of frozen sections after immunofluorescence staining. (**C**) R-Ras is expressed in the endothelial cells in the retina and (**D**) also in the preretinal blood vessels. (**E**) Some of the preretinal blood vessels are negative for R-Ras. (**F**) R-Ras is expressed in the pericytes (NG2, *red*) in the retina. Some pericytes of preretinal blood vessels are negative for R-Ras in OIR (*arrow*), but (**G**) R-Ras is also expressed in the pericytes of preretinal neovessels. *Scale bars*: 100 μm (**A**, **B**), 20 μm (**C–G**).

influence on development of retinal vasculature by R-Ras is in line with the above-reported low expression of R-Ras at the early stages of retinal vascular development (Supplementary Fig. S1).

Induction and Selective Disappearance of R-Ras From the Pathologic Neovasculature in OIR

Next, the R-Ras expression profile in the OIR model was analyzed using WT mice. Using qPCR, a 2.5-fold increase of *Rras* mRNA from normal P17 to P17 OIR model retinas was detected. Using Western blot analysis, a 7.5-fold increase in R-Ras protein levels was seen in OIR P17 retinas compared to healthy P17 retinas. At P12, the expression of R-Ras was reduced in OIR. The amount of R-Ras expression is in line with regression of the vasculature at P12 and vessel regrowth at P17 in the OIR model (Fig. 1). Using R-Ras immunohistochemistry, R-Ras was found to be localized mainly to the blood vessels in OIR retinas (Fig. 2, Supplementary Fig. S4). A faint R-Ras expression was also detected outside of the retinal blood vessels in mouse retina (Fig. 2A). This immunohistochemical signal most probably represents low expressions from retinal neuronal cells, which are known to express R-Ras.[35] Using R-Ras and endothelial cell (CD31), as well as R-Ras and pericyte (NG2), double-staining, R-Ras expression was shown to be confined to endothelial cells and pericytes in retinal vessels (Fig. 2). It appeared that all of the retinal blood vessels expressed R-Ras, whereas only 68% of the preretinal neovessels had R-Ras expression at P17 in the OIR model (Fig. 2A, Supplementary Fig. S4). This finding was confirmed by double immunofluorescent imaging of the retina showing some preretinal neovessels devoid of R-Ras expression in OIR (Figs. 2E, 2F). By costaining the retinal tissue sections for R-Ras and endothelial cells, as well as for R-Ras and pericytes, the R-Ras expression was confirmed to be confined to both endothelial cells and pericytes (Figs. 2B–G).

Investigative Ophthalmology & Visual Science

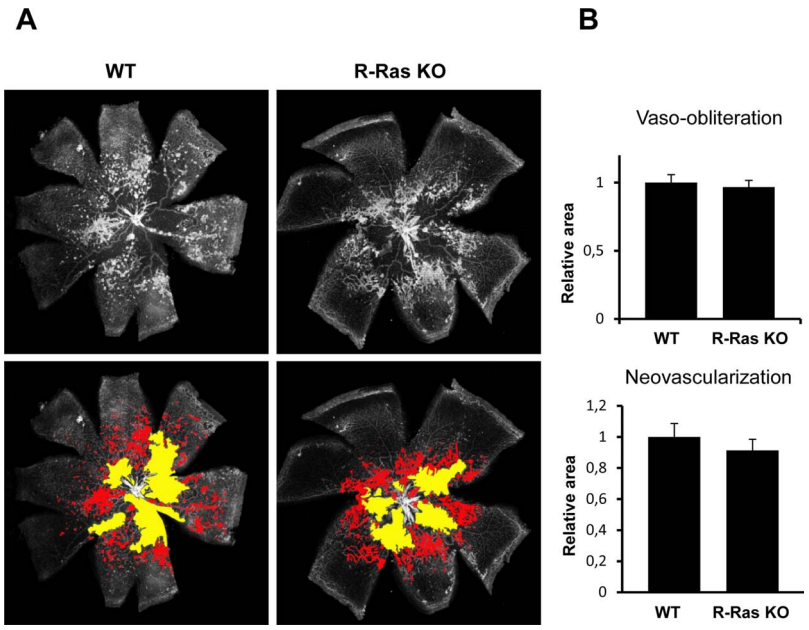

Figure 3. Neither revascularization nor pathologic neovascularization is affected by R-Ras deficiency in the OIR model. Wild-type and R-Ras KO mice pups were exposed to hyperoxia as previously described, and retinas were harvested at P17. Areas of vascular obliteration and pathologic neovascularization (meaning neovascular tufts) were quantified from Isolectin IB_4–stained whole mounts using Adobe Photoshop CS3. (**A**) Representative retinas of WT and R-Ras KO mice at P17. The revascularization rate was determined by quantifying the avascular areas (*yellow*) in retinal flat mounts. The amount of pathologic neovascularization (tufts, *red*) was also determined. (**B**) Summary of quantitative analysis of vascular obliteration (*yellow*) and neovascularization (*red*). The avascular and pathologic neovascularization areas were measured, and results are represented as an area relative to WT area. *Error bars* represent ± 95% confidence intervals. (WT: $n = 63$, KO: $n = 48$ retinas.)

R-Ras Does Not Change the Hypoxic Revascularization Rate of the Retina

As all of the antiangiogenic molecules used to treat neovascular retinal diseases have been shown to inhibit sprouting angiogenesis induced in the OIR model,[36–38] the role of R-Ras in hypoxia-driven neovascularization in the retina was explored next. First, we determined whether regression of vessels under hyperoxic conditions in the OIR model is comparable between R-Ras KO and WT mice. After exposure to 75% oxygen between P7 and P12, retinas were evaluated at P12. Typical for this model,[39] large areas of the central vascular network were obliterated, with only a few major vessels remaining centrally in both WT and R-Ras KO mice (Supplementary Fig. S5). Quantitative analysis of obliterated areas in retina confirmed that the retinal vasculature in R-Ras KO and WT mice are affected in a similar fashion by hyperoxic exposure (Supplementary Fig. S5). Taken together, these data suggest that deletion of R-Ras has no observable effect on vascular regression and remodeling in the retina in response to hyperoxic conditions.

On return to normoxia, the avascular and hypoxic central retina stimulates rapid regrowth of vessels.[24] The rate of retinal revascularization in WT and R-Ras KO retinas was determined by quantifying avascular retinal area 5 days after the mice were returned to normoxia. There was no significant difference in the avascular retinal area between the WT and R-Ras KO, indicating that the rate of retinal revascularization is similar between the WT and R-Ras KO mice at P17 (Fig. 3). In addition to revascularization of the retina, the strong hypoxic stimulus from the center of the retina also drives abnormal misdirected sprouting of blood vessels into the vitreous at the interface between the centrally obliterated and peripherally perfused retina.[24] Preretinal (i.e., pathologic) neovascularization reaches its maximum in WT mice 5 days after returning to normoxia (at P17).[24] No significant differences in the number of preretinal neovascular tufts and clusters were found between R-Ras KO mice and WT mice (Fig. 3). The results indicate that neither the hypoxia-induced revascularization rate of the obliterated areas in retina nor the rate of preretinal neovascularization is affected by R-Ras deletion.

R-Ras Deficient Retinal Blood Vessels Have Increased Permeability in OIR

It has been recently shown that loss of R-Ras worsens blood vessel structure and perfusion and the pathologic plasma leakage in tumor angiogenesis.[15,21] In order to assess the role of R-Ras in controlling the vascular permeability of the retinal vasculature, the OIR model was used. The vascular leakage was quantified by measuring EB dye extravasation from retinal vessels. The R-Ras KO retinas had approximately 100% increase in the retinal EB leakage compared with the WT retinas in OIR ($P = 0.0223$ at 1 hour and $P = 0.0006$ at 24 hours; Figs. 4A–C). No difference was detected in the amount of EB leakage when comparing normal WT and R-Ras KO retinas (Supplementary Fig. S6). To confirm the enhanced retinal leakage in R-Ras KO animals in OIR, we also measured the amount of IgG heavy chain molecule accumulation in the retina, as this antibody subclass is normally compartmentalized within the circulation.[40] We could not detect a difference in IgG leakage in the normal retinas between WT and R-Ras KO animals. A 4-fold increase in the amount of IgG was detected in the R-Ras KO retinas over the WT retinas in OIR as a sign of increased vascular permeability ($P = 0.0007$; Fig. 4D). To rule out the possibility that the increased levels of IgG in the R-Ras KO OIR retinas were due to plasma cells, immunohistologic staining of CD138/Syndecan-1 was performed. There was no increase in the number of plasma cells in KO retinas compared to WT in the OIR samples (Supplementary Fig. S7).

Investigative Ophthalmology & Visual Science

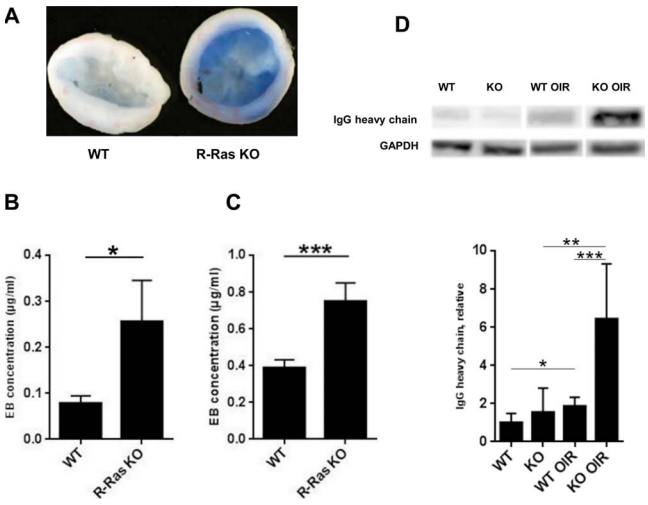

Figure 4. R-Ras deficiency increases vessel permeability in mouse OIR model. Wild-type and R-Ras KO mice pups were exposed to hyperoxia as described previously. The EB dye was injected IP, and retinas and blood samples were harvested after 1 hour and 24 hours at P17. Evans Blue concentrations were measured spectrophotometrically at 620 nm, and EB concentration for each sample was calculated from a standard curve. Results are expressed as relative to EB concentration in the plasma. (**A**) Representative R-Ras KO and WT OIR retinas after systemic injection of EB dye. In many of the R-Ras KO retinas, EB dye was visible, whereas most of the WT retinas were colorless. (**B**) Statistical analysis of a representative experiment shows a significant increase in vascular leakage in R-Ras KO OIR retinas compared to WT OIR retinas already at a 1-hour time point ($P = 0.0223$, *, nonparametric Mann-Whitney U test, WT $n = 6$, R-Ras KO $n = 8$). (**C**) There is a highly significant difference in vascular leakage between R-Ras KO and WT mice at the 24-hour time point ($P = 0.0006$, ***, nonparametric Mann-Whitney U test; WT $n = 20$, R-Ras KO $n = 18$). *Error bars* represent SEM. To assess the IgG protein accumulation, OIR retinas were harvested at P17, proteins were extracted and samples were electrophoresed on gradient gels, and Western blotting was done using anti-mouse IgG antibody. (**D**) Representative images of immunoblotting from where mouse IgG heavy chain densities were quantified and normalized against GAPDH. Relative comparison of IgG heavy chain protein from WT OIR and R-Ras KO OIR samples gives a 3.5-fold difference ($P = 0{,}0007$, ***, nonparametric Mann-Whitney U test). There is no difference in the IgG protein level between healthy WT and KO mice at P17 ($P = 0.7879$). *Error bars* represent ± 95% confidence intervals. (WT: $n = 6$, KO: $n = 6$, WT OIR: $n = 14$, KO OIR: $n = 16$.)

R-Ras Deficiency Severely Impairs Pericyte Coverage of Angiogenic Blood Vessels and Reduces VE-Cadherin Expression in OIR Model

Close interaction between sprouting endothelium and pericytes is crucial for vessel maturation and stability.[41,42] Pathologic, angiogenic vasculature in tumors is characterized by insufficient pericyte association around the blood vessels.[43] Consistent with this notion, a significant reduction in the direct physical contact between pericytes and the endothelium of blood vessels was found in R-Ras KO retinas in the OIR model at P17 (Figs. 5A–B). When the pericyte coverage around the tips of the sprouting angiogenic blood vessels was quantified, 40% reduction in the pericyte coverage was recorded in the R-Ras KO retinas over the WT retinas ($P = 0.033$; Fig. 5C).

Vascular endothelial–cadherin is a member of cadherin superfamily expressed exclusively on endothelial cells.[21] It is a crucial factor of adherens junctions between the endothelial cells.[15] R-Ras is known to stabilize adherens junctions by inhibiting VEGF-induced VE-cadherin internalization.[15] We studied the expression of VE-cadherin in OIR model, and we observed that both the intensity of the VE-cadherin immunostaining and colocalization of VE-cadherin with CD31 were significantly reduced in KO mice compared to WT mice (Fig. 5D). Colocalization analysis showed significant reduction in VE-cadherin and CD31 colocalization in R-Ras KO mice compared to WT mice (overlap coefficient according to Manders: $r = 0.51$ for WT, and $R = 0.43$ for KO ($P = 0.04$)). Our finding on VE-cadherin expression is in line what has been reported in tumor vasculature of R-Ras KO and WT mice.[21]

Reduced R–Ras Expression in the Neovessels of Human Diabetic Retinopathy Correlates With Increased Vascular Leakage and the Immature State of the Neovessels

R-Ras expression was restricted exclusively to blood vessels in normal human retina, and it was expressed in all blood vessels in normal human retinas (Supplementary Fig. S8). To address the relevance of our findings on the role of R-Ras in the OIR model to human ischemic retinopathies, the pathologic retinal neovascular membranes that develop in human diabetic retinopathy patients were studied. These neovascular membranes were collected from patients suffering from type I diabetes, who had already developed tractional retinal detachment due to fibrosis of neovascular membranes. Thus, the samples represent the end stage of the disease, where substantial amount of fibrosis is associated with neovessels, but they still contain regions with active pathologic angiogenesis. In the diabetic neovascular membranes, R-Ras expression was exclusively restricted to blood vessels (Fig. 6). Like pathologic preretinal neovessels in the OIR model, human diabetic neovascular membranes had varying expression of R-Ras (Fig. 6). Only approximately 80% of the blood vessels in the human neovascular membranes expressed any R-Ras protein at all (Fig. 6C). To explore whether R-Ras expression has any relation to the blood vessel maturity, the human tissue samples were double-stained for R-Ras and VEGFR2, a marker of blood vessel immaturity.[44,45] A strong inverse correlation between expression of the two proteins was identified (Spearman's $\rho = -0.821$, $P = 0.023$, $R^2 = 0.563$); the higher the percentage of immature blood vessels (VEGFR2+), the less R-Ras expression there was in the blood vessels (Fig. 6).

To address whether lack of R-Ras in immature blood vessels influences vascular permeability in human diabetic neovascular membranes, samples were stained for HSA. Samples with a low percentage of R-Ras–expressing blood vessels showed a strong accumulation of HSA outside the vessels, whereas samples with a high percentage of R-Ras–expressing blood vessels had HSA staining restricted mainly inside the vessels (Figs. 6A–B). There was a strong negative correlation between area of extravascular HSA and the number of R-Ras–positive vessels (Spearman's ρ: $r = -0.886$, $P = 0.019$, $R^2 = 0.835$); the more vascular leakage outside of the blood vessels, the less R-Ras expression was in the blood vessels. Furthermore, we could demonstrate that leaked, extravascular HSA was detected mainly around individual blood vessels that lack R-Ras (Fig. 7). This was especially evident in samples that had R-Ras in the majority of blood vessels as extravascular HSA mainly accumulated around those few blood vessels devoid of R-Ras expression (Fig. 7).

Discussion

The present study demonstrates that the small GTPase R-Ras regulates the pathologic permeability of blood vessels in hypoxia-driven angiogenesis without altering the rate of

Investigative Ophthalmology & Visual Science

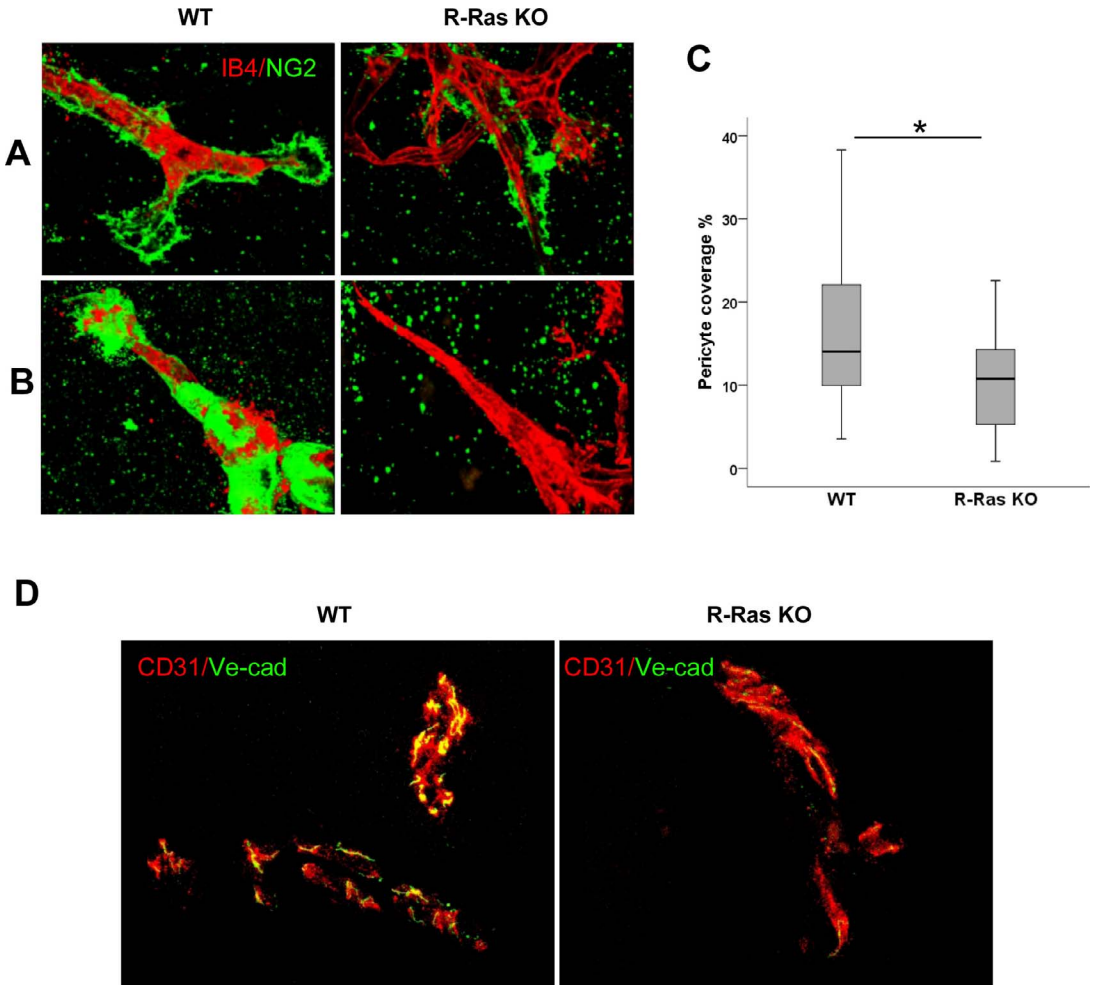

Figure 5. Pericyte coverage and VE-cadherin expression is reduced in R-Ras KO in the OIR model in angiogenic retinal blood vessels. Oxygen-induced retinopathy was induced in WT and R-Ras KO mice as described previously. Retinas were harvested at P17, and whole-mount retinas were double-stained with Alexa Fluor–conjugated Isolectin IB_4 and with an antibody against the pericyte marker NG2 proteoglycan. Three-dimensional images were taken from the most superficial vascular plexus at the tips of the blood vessels from the region where vessels grow toward the optic nerve. (**A**) Representative images of WT and R-Ras KO blood vessel endothelial cells (*red*) surrounded by pericytes (*green*). (**B**) The majority of images from WT mice retina had a lot of pericytes around the blood vessels, whereas the majority of pictures taken from the KO retinal blood vessels were lacking or had very few pericytes. (**C**) Direct contact between endothelial cells and pericytes was quantified by colocalization analysis. The result is shown as a percentage of endothelial cell area colocalized with pericytes in WT and R-Ras KO retinal blood vessel tips. The pericyte coverage is significantly reduced in R-Ras KO animals compared to WT by 40% ($P = 0.033$, *). *Error bars* represent ± 95% confidence intervals. (WT: $n = 15$; R-Ras KO: $n = 15$. Two pictures were taken from each retina, and an average was calculated). The expression of VE-cadherin was studied in the OIR model by staining frozen cross-sections of retina with antibodies against VE-cadherin and endothelial cells (CD31). The intensity as well as the colocalization of VE-cadherin staining with endothelial cells was quantified using BioImageXD. (**D**) Representative images of VE-cadherin (*green*) and CD31 (*red*) in P17 OIR model in WT and R-Ras KO are presented. Colocalization analysis showed significant reduction in VE-cadherin and CD31 colocalization in R-Ras KO mice compared to WT mice (overlap coefficient according to Manders: $r = 0.51$ for WT and $R = 0.43$ for KO [$P = 0.04$]), $n = 5$ mice for WT and $n = 5$ mice for KO.

revascularization of the hypoxic retina. Furthermore, by analyzing a set of preretinal vascular membranes obtained from diabetic retinopathy patients, we were able to demonstrate that neovascular membranes with reduced R-Ras expression in immature vessels display increased pathologic vascular leakage. Given that increased vascular leakage is the pathognomonic feature in human diabetic retinopathy, our study implicates that loss of R-Ras may have a pathologic role in this disease.

R-Ras reduced the pathologic vascular permeability in ischemia-induced retinopathy without inhibiting retinal angiogenesis, whether it was developmental or induced by hypoxia in OIR. This is a clear difference to all current available antiangiogenic therapies that have been shown to function in OIR by inhibiting sprouting angiogenesis.[36] Furthermore, the mechanism of resistance to the currently available antiangiogenic therapies both in tumors and retinopathy is actually related to the eradication of the neovessels, which, in turn, worsens the underlying ischemia and drives the formation of new, leaky blood vessels by alternative molecular mechanism.[13] Thus, the proposed molecular mechanism for future antiangiogenic therapies is one in which the angiogenic blood vessels are "normalized" to stable ones to alleviate the hypoxia and stop the detrimental aberrant vascular leakage.[46,47] Taken with earlier demonstrations of a causal relationship between R-Ras expression and vessel maturation,[15,20,48,49] our results suggest potential utility of R-Ras in treating retinopathies involving angiogenesis. Modulating R-Ras expression repre-

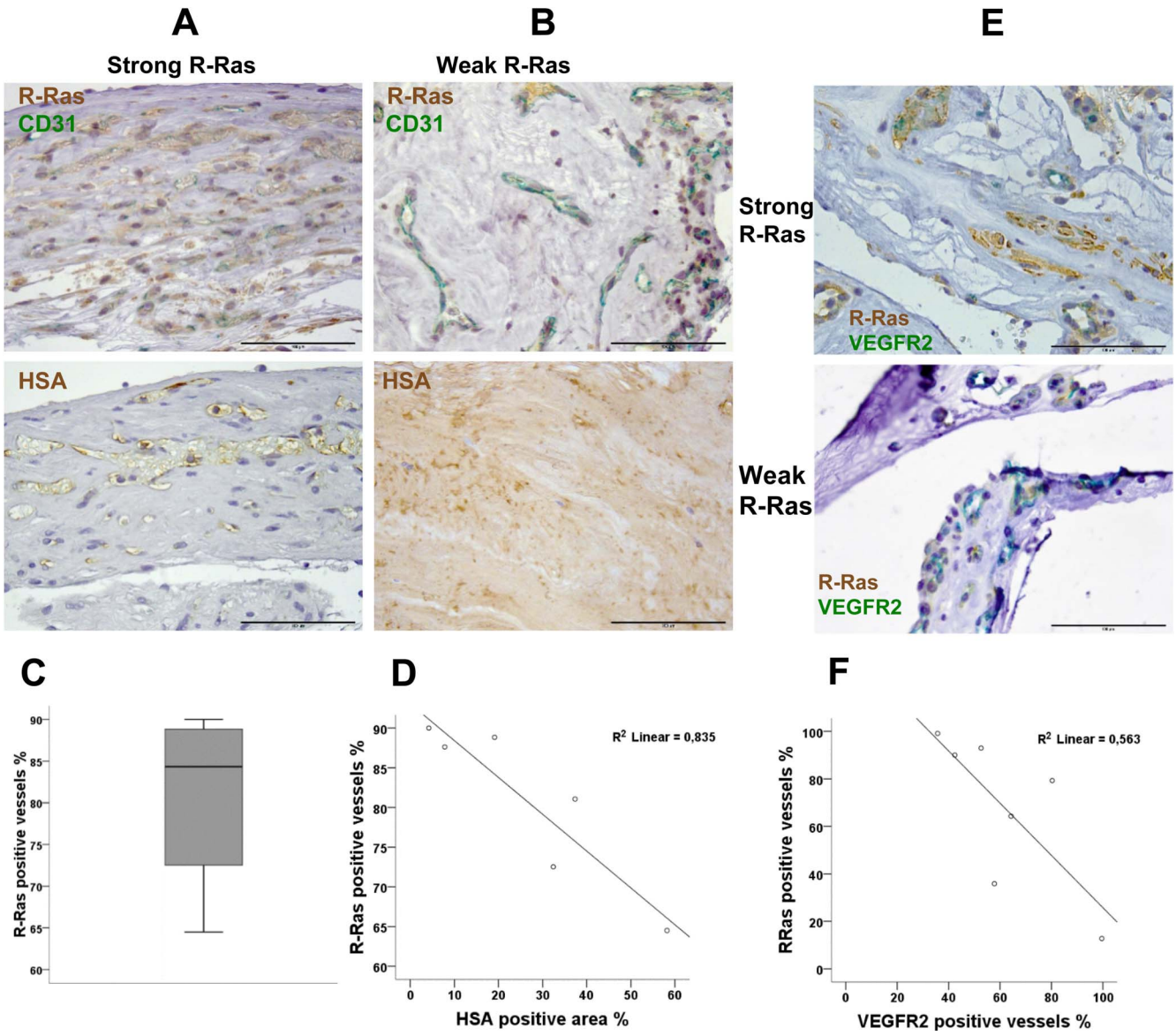

Figure 6. Reduced R-Ras expression correlates with leakage of human serum albumin in human diabetic retinopathy vasculature, and it is negatively correlated with VEGFR2 expression. Preretinal neovascular membranes obtained from vitrectomies from diabetic retinopathy patients were analyzed by immunohistochemistry for their protein expression. Immunohistochemical staining from adjacent sections was done with anti-CD31 + anti–R-Ras, anti-HSA, and anti–R-Ras + anti-VEGFR2 antibodies. The number of R-Ras–positive vessels was calculated from R-Ras and CD31 double-stained sections ($n = 7$; 5–9 different sections analyzed from each sample). Correlation analysis between R-Ras and VEGFR2 was done from R-Ras + VEGFR2 double-stained sections and compared to CD31 staining from adjacent sections ($n = 7$; 5–9 different sections analyzed from each sample). Vascular membranes with strong R-Ras expression show limited extravascular staining for HSA (**A**), whereas samples with weak R-Ras expression show strong staining for HSA outside the blood vessels (**B**). *Scale bars*: 100 μm. There is a strong inverse correlation between HSA-positive extravascular area and the percentage of R-Ras–positive neovessels (Spearman's ρ: $r = -0.886$, $P = 0.019$, *, $R^2 = 0.835$, $n = 6$ patients) (**D**). (**C**) Approximately 20% of the neovessels do not express any R-Ras at all (R-Ras–positive vessels 81 ± 10%, mean + SD, $n = 6$ patients). Data are shown as a box plot with median and 95% confidence interval. (**E**, **F**) Double-staining for R-Ras and VEGFR2 shows an inverse correlation (Spearman's ρ: $r = -0.821$, $P = 0.023$, $R^2 = 0.563$) between the number of R-Ras–expressing and VEGFR2-positive blood vessels. When a majority of blood vessels has R-Ras expression, a majority of blood vessels are negative for VEGFR2 expression, whereas the VEGFR2 expression is opposite when very few blood vessels express R-Ras. *Scale bars*: 200 μm.

sents a novel therapeutic approach that may be capable of addressing pathologic vascular permeability without simultaneously worsening the underlying pathobiology of the disease— hypoxia.

The differences between the mechanisms of R-Ras and other antiangiogenic therapies are evidenced by a recent report implicating activated Ras signaling as a key mediator of pathologic neovascularization induced by many cytokines and growth factors, including VEGF, in blinding neovascular eye diseases.[22] Westenskow et al.[22] reported that aberrant Ras signaling can be inhibited by a molecule called p120RasGAP. The inhibitory function of p120RasGAP on Ras-driven retinal neovascularization was shown to take place through the inhibition of sprouting angiogenesis.[22] In contrast, R-Ras functions in the retina primarily to stabilize vasculature and prevent leakage and does not inhibit sprouting angiogenesis in OIR. The mechanistic differences between R-Ras and p120Ras-

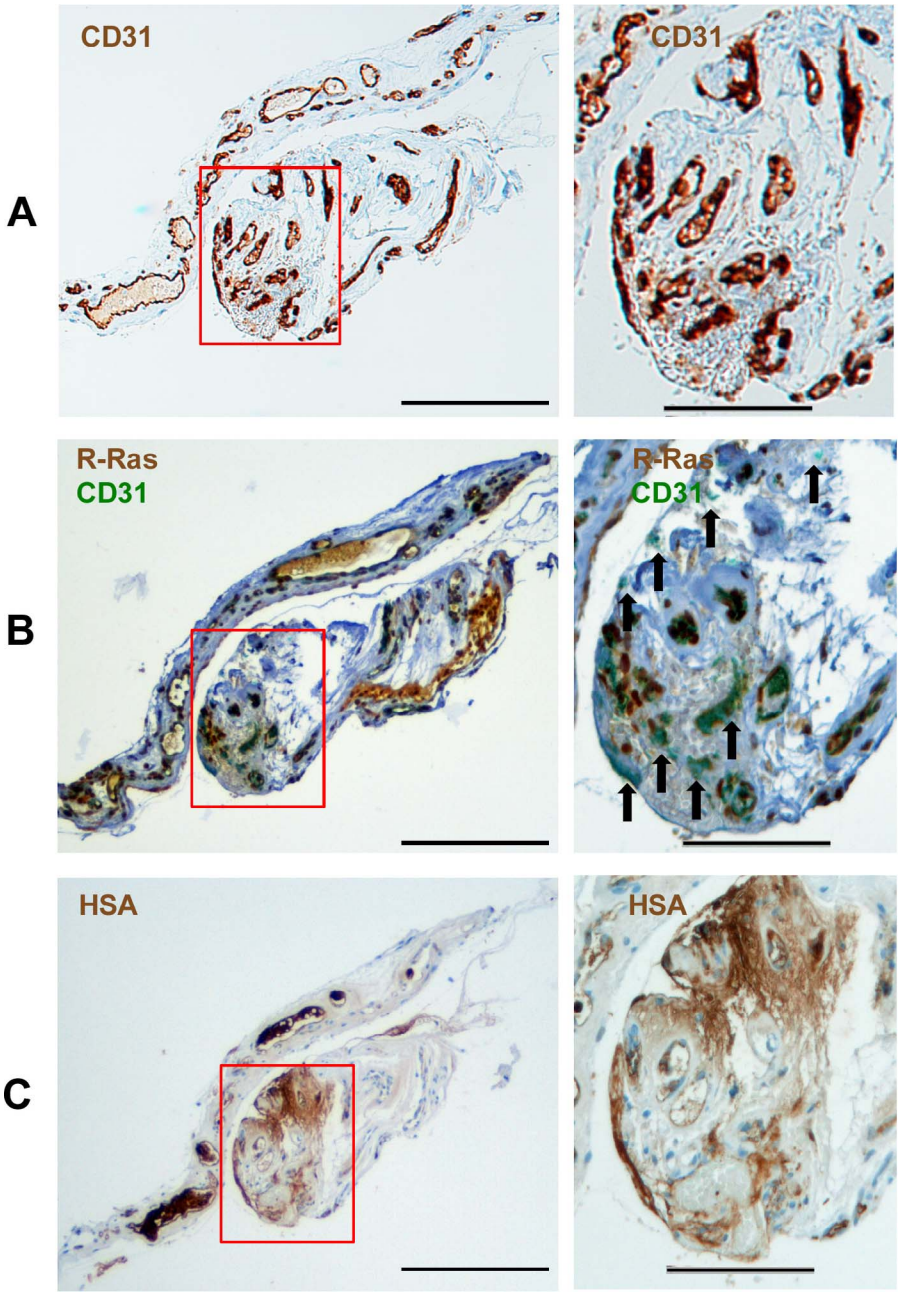

Figure 7. Vascular leakage is mainly from blood vessels that do not express R-Ras in human diabetic retinopathy**.** The preretinal membranes from human diabetic retinopathy patients were either stained for CD31, double-stained for CD31 (*green*) and R-Ras (*brown*) or stained for HSA (*brown*). (**A**) Blood vessels in preretinal membranes stained for endothelial cells (CD31, *brown*). (**B**) Double-staining of blood vessels (CD31, *green*) and R-Ras (*brown*) expression. (**C**) Vascular leakage was determined by using an antibody against HSA (*brown*). Red boxes on figures on the left are presented as high magnification pictures on the right. (**B** and **C**) No vascular leakage (restricted HSA staining only inside the neovessels) can be seen around neovessels with strong R-Ras expression. Conversely, the blood vessels that do not express any R-Ras show aberrant vascular permeability around them. *Arrows* represent R-Ras–negative blood vessels. *Scale bars* on the left represent 450 μm and 200 μm on the right.

GAP are further highlighted by the fact that p120RasGAP actually inhibits R-Ras.[50]

R-Ras has recently been proposed as a master regulator of transendothelial permeability in angiogenesis.[15,21,51] Our understanding of the molecular mechanisms by which R-Ras exerts its biological effects on endothelial cells has increased recently.[15,48] It has been demonstrated that R-Ras suppresses endothelial cells' response to VEGF by inhibiting internalization of VEGFR2 that is required for full activation of the receptor[49] as well as by inhibiting VEGFR2-p38MAPK-HSP27 signaling axis.[51] However, the biological effects of R-Ras in angiogenesis cannot be solely attributed to the inhibition of the VEGF signaling because VEGF inhibitors have been shown to function in OIR by inhibiting sprouting angiogenesis,[36,37] whereas R-Ras is known to promote endothelial cell survival.[20] In addition to the inhibition of VEGF, it has been demonstrated that R-Ras forms a complex with Rab interactor 2 protein and Rab5, and then this complex activate Rac1, which in turn activates integrins to promote endothelial cell adhesion to surrounding ECM.[52,53] R-Ras also interacts with filamin A,

which is crucial for maintaining of endothelial barrier function.[54] Furthermore, actin-binding protein Girdin/GIV regulates transendothelial permeability by controlling VE-cadherin trafficking through R-Ras.[48] In the present study, we confirmed a previous finding that R-Ras is required for recruitment of pericytes around endothelial cells,[21] which is crucial for blood vessel stabilization.[41] In accordance with previous studies on tumors, we demonstrated that R-Ras deficiency reduces VE-cadherin expression in endothelial cells, which may result in increased vessel leakiness in R-Ras–deficient mice.[21]

We demonstrate that angiogenic blood vessels, especially immature VEGFR2+ vessels, show reduced expression of R-Ras in human diabetic neovascular membranes, and the reduced R-Ras expression correlates with increased vascular leakage from the neovessels of human diabetic vasculature. We suggest that reduced vascular R-Ras expression is a critical feature in the pathogenesis of human diabetic retinopathy, especially in the accumulation of retinal edema. Thus, R-Ras represents a promising new therapeutic target to address angiogenesis-related pathologic vascular permeability.

Acknowledgments

The authors thank Anni Laitinen, Marianne Karlsberg, and Marja-Leena Koskinen for excellent technical assistance; Erkki Ruoslahti (Sanford Burnham Prebys Medical Discovery Institute, La Jolla, CA, USA) for providing the R-Ras knockout mice for the study and for his thoughtful comments on the manuscript; and William B. Stallcup (Sanford Burnham Prebys Medical Discovery Institute, La Jolla, CA, USA) for providing the NG2 antibody. The work was supported by the Sigrid Juselius Foundation, the Academy of Finland, Päivikki and Sakari Sohlberg Foundation, Instrumentarium Research Foundation, Finnish Medical Foundation, Pirkanmaa Hospital District Research Foundation, the Finnish Cultural Foundation, Finnish Diabetic Research Foundation, Diabetes Wellness Foundation, Tampere Tuberculosis Foundation, Finnish Eye Foundation, National Institute of Health Grant CA125255, National Science Foundation Grant CBET-1403535, and Florida Department of Health, Bankhead Coley Cancer Program Grant 4BB17, and the Mary and Georg Ehrnrooth Foundation.

Disclosure: **M. Vähätupa**, None; **S. Prince**, None; **S. Vataja**, None; **T. Mertimo**, None; **M. Kataja**, None; **K. Kinnunen**, None; **V. Marjomäki**, None; **H. Uusitalo**, None; **M. Komatsu**, None; **T.A.H. Järvinen**, None; **H. Uusitalo-Järvinen**, None

References

1. Ferrara N, Davis-Smyth T. The biology of vascular endothelial growth factor. *Endocr Rev*. 1997;18:4–25.
2. Keck PJ, Hauser SD, Krivi G, et al. Vascular permeability factor, an endothelial cell mitogen related to PDGF. *Science*. 1989; 246:1309–1312.
3. Vinores SA, Chan CC, Vinores MA, et al. Increased vascular endothelial growth factor (VEGF) and transforming growth factor beta (TGFbeta) in experimental autoimmune uveoretinitis: upregulation of VEGF without neovascularization. *J Neuroimmunol*. 1998;89:43–50.
4. Ford JA, Lois N, Royle P, Clar C, Shyangdan D, Waugh N. Current treatments in diabetic macular oedema: systematic review and meta-analysis. *BMJ Open*. 2013;3:e002269.
5. Arevalo JF, Maia M, Flynn HW Jr, et al. Tractional retinal detachment following intravitreal bevacizumab (Avastin) in patients with severe proliferative diabetic retinopathy. *Br J Ophthalmol*. 2008;92:213–216.
6. Moradian S, Ahmadieh H, Soheilian M, Dehghan MH, Azarmina M. Intravitreal bevacizumab in active progressive proliferative diabetic retinopathy. *Graefes Arch Clin Exp Ophthalmol*. 2008;246:1699–1705.
7. Chakravarthy U, Harding SP, Rogers CA, et al.; and the IVAN Study Investigators. Ranibizumab versus bevacizumab to treat neovascular age-related macular degeneration: one-year findings from the IVAN randomized trial. *Ophthalmology*. 2012; 119:1399–1411.
8. Matsuyama K, Ogata N, Matsuoka M, Wada M, Takahashi K, Nishimura T. Plasma levels of vascular endothelial growth factor and pigment epithelium-derived factor before and after intravitreal injection of bevacizumab. *Br J Ophthalmol*. 2010; 94:1215–1218.
9. Petrou P, Georgalas I, Giavaras G, Anastasiou E, Ntana Z, Petrou C. Early loss of pregnancy after intravitreal bevacizumab injection. *Acta Ophthalmol*. 2010;88(4):e136.
10. Chen HX, Cleck JN. Adverse effects of anticancer agents that target the VEGF pathway. *Nat Rev Clin Oncol*. 2009;6:465–477.
11. Nazer B, Humphreys BD, Moslehi J. Effects of novel angiogenesis inhibitors for the treatment of cancer on the cardiovascular system: focus on hypertension. *Circulation*. 2011;124:1687–1691.
12. Anderson OA, Bainbridge JW, Shima DT. Delivery of anti-angiogenic molecular therapies for retinal disease. *Drug Discov Today*. 2010;15:272–282.
13. Manousaridis K, Talks J. Macular ischaemia: a contraindication for anti-VEGF treatment in retinal vascular disease? *Br J Ophthalmol*. 2012;96:179–184.
14. Lowe DG, Capon DJ, Delwart E, Sakaquchi AY, Naylor SL, Goeddel DV. Structure of the human and murine R-ras genes, novel genes closely related to ras proto-oncogenes. *Cell*. 1987; 48:137–146.
15. Sawada J, Komatsu M. Normalization of tumor vasculature by R-Ras. *Cell Cycle*. 2012;11:4285–4286.
16. Lowe DG, Goeddel DV. Heterologous expression and characterization of the human R-ras gene product. *Mol Cell Biol*. 1987;7:2845–2856.
17. Zhang Z, Vuori K, Wang H, Reed JC, Ruoslahti E. Integrin activation by R-ras. *Cell*. 1996;85:61–69.
18. Suzuki J, Kaziro Y, Koide H. Positive regulation of skeletal myogenesis by R-Ras. *Oncogene*. 2000;19:1138–1146.
19. Ehrhardt A, Ehrhardt GR, Guo X, Schrader JW. Ras and relatives—job sharing and networking keep an old family together. *Exp Hematol*. 2002;30:1089–1106.
20. Komatsu M, Ruoslahti E. R-Ras is a global regulator of vascular regeneration that suppresses intimal hyperplasia and tumor angiogenesis. *Nat Med*. 2005;11:1346–1350.
21. Sawada J, Urakami T, Li F, et al. Small GTPase R-Ras regulates integrity and functionality of tumor blood vessels. *Cancer Cell*. 2012;22:235–249.
22. Westenskow PD, Kurihara T, Aquilar E, et al. Ras pathway inhibition prevents neovascularization by repressing endothelial cell sprouting. *J Clin Invest*. 2013;123:4900–4908.
23. Smith LE, Wesolowski E, McLellan A, et al. Oxygen-induced retinopathy in the mouse. *Invest Ophthalmol Vis Sci*. 1994;35: 101–111.
24. Uusitalo-Jarvinen H, Kurokawa T, Mueller BM, Andrade-Gordon P, Friedlander M, Ruf W. Role of protease activated receptor 1 and 2 signaling in hypoxia-induced angiogenesis. *Arterioscler Thromb Vasc Biol*. 2007;27:1456–1462.
25. Stahl A, Chen J, Sapieha P, et al. Postnatal weight gain modifies severity and functional outcome of oxygen-induced proliferative retinopathy. *Am J Pathol*. 2010;177:2715–2723.
26. Huang FJ, You WK, Bonaldo P, Seyfried TN, Pasquale EB, Stallcup WB. Pericyte deficiencies lead to aberrant tumor vascularizaton in the brain of the NG2 null mouse. *Dev Biol*. 2010;344:1035–1046.

27. Kankaanpaa P, Paavolainen L, Tiitta S, et al. BioImageXD: an open, general-purpose and high-throughput image-processing platform. *Nat Methods*. 2012;9:683–689.
28. Livak KJ, Schmittgen TD. Analysis of relative gene expression data using real-time quantitative PCR and the 2(-Delta C(T)) method. *Methods*. 2001;25:402–408.
29. Scheppke L, Aguilar E, Gariano RF, et al. Retinal vascular permeability suppression by topical application of a novel VEGFR2/Src kinase inhibitor in mice and rabbits. *J Clin Invest*. 2008;118:2337–2346.
30. Xu Q, Qaum T, Adamis AP. Sensitive blood-retinal barrier breakdown quantitation using Evans blue. *Invest Ophthalmol Vis Sci*. 2001;42:789–794.
31. May U, Prince S, Vahatupa M, et al. Resistance of R-Ras knockout mice to skin tumour induction. *Sci Rep*. 2015;5: 11663.
32. Fruttiger M. Development of the retinal vasculature. *Angiogenesis*. 2007;10:77–88.
33. Stahl A, Connor KM, Sapieha P, et al. The mouse retina as an angiogenesis model. *Invest Ophthalmol Vis Sci*. 2010;51: 2813–2826.
34. Ehling M, Adams S, Benedito R, Adams RH. Notch controls retinal blood vessel maturation and quiescence. *Development*. 2013;140:3051–3061.
35. Ivins JK, Yurchenco PD, Lander AD. Regulation of neurite outgrowth by integrin activation. *J Neurosci*. 2000;20:6551–6560.
36. Hollanders K, Van Bergen T, Van de Velde S, Stalmans I. Bevacizumab revisited: its use in different mouse models of ocular pathologies. *Curr Eye Res*. 2014;40:1–11.
37. Sone H, Kawakami Y, Segawa T, et al. Effects of intraocular or systemic administration of neutralizing antibody against vascular endothelial growth factor on the murine experimental model of retinopathy. *Life Sci*. 1999;65:2573–2580.
38. Tokunaga CC, Mitton KP, Dailey W, et al. Effects of anti-VEGF treatment on the recovery of the developing retina following oxygen-induced retinopathy. *Invest Ophthalmol Vis Sci*. 2014; 55:1884–1892.
39. Connor KM, Krah NM, Dennison RJ, et al. Quantification of oxygen-induced retinopathy in the mouse: a model of vessel loss, vessel regrowth and pathological angiogenesis. *Nat Protoc*. 2009;4:1565–1573.
40. Mayumi M, Kuritani T, Kubagawa H, Cooper MD. IgG subclass expression by human B lymphocytes and plasma cells: B lymphocytes precommitted to IgG subclass can be preferentially induced by polyclonal mitogens with T cell help. *J Immunol*. 1983;130:671–677.
41. Hellström M, Gerhardt H, Kalén M, et al. Lack of pericytes leads to endothelial hyperplasia and abnormal vascular morphogenesis. *J Cell Biol*. 2001;153:543–553.
42. Uemura A, Ogawa M, Hirashima M, et al. Recombinant angiopoietin-1 restores higher-order architecture of growing blood vessels in mice in the absence of mural cells. *J Clin Invest*. 2002;110:1619–1628.
43. Jain RK. Molecular regulation of vessel maturation. *Nat Med*. 2003;9:685–693.
44. Heidenreich R, Kappel A, Breier G. Tumor endothelium-specific transgene expression directed by vascular endothelial growth factor receptor-2 (Flk-1) promoter/enhancer sequences. *Cancer Res*. 2000;60:6142–6147.
45. Kappel A, Ronicke V, Damert A, Flamme I, Risau W, Breier G. Identification of vascular endothelial growth factor (VEGF) receptor-2 (Flk-1) promoter/enhancer sequences sufficient for angioblast and endothelial cell-specific transcription in transgenic mice. *Blood*. 1999;93:4284–4292.
46. Jain RK. Antiangiogenesis strategies revisited: from starving tumors to alleviating hypoxia. *Cancer Cell* 2014;26:605–622.
47. McIntyre A, Harris AL. Metabolic and hypoxic adaptation to anti-angiogenic therapy: a target for induced essentiality. *EMBO Mol Med*. 2015:7;368–379.
48. Ichimiya H, Maeda K, Enomoto A, Weng L, Takahashi M, Murohara T. Girdin/GIV regulates transendothelial permeability by controlling VE-cadherin trafficking through the small GTPase, R-Ras. *Biochem Biophys Res Commun*. 2015;461: 260–267.
49. Sawada J, Li F, Komatsu M. R-Ras protein inhibits autophosphorylation of vascular endothelial growth factor receptor 2 in endothelial cells and suppresses receptor activation in tumor vasculature. *J Biol Chem* 2015;290:8133–8145.
50. Dail M, Richter M, Godement P, Pasquale B. Eph receptors inactivate R-Ras through different mechanisms to achieve cell repulsion. *J Cell Sci*. 2006;119:1244–1254.
51. Sawada J, Li F, Komatsu M. R-Ras inhibits VEGF-induced p38MAPK activation and HSP27 phosphorylation in endothelial cells. *J Vasc Res*. 2015;52:347–359.
52. De Franceschi N, Hamidi H, Alanko J, Sahgal P, Ivaska J. Integrin traffic—the update. *J Cell Sci*. 2015;128;839–852.
53. Sandri C, Caccavari F, Valdembri D, et al. The R-Ras/RIN2/Rab5 complex controls endothelial cell adhesion and morphogenesis via active integrin endocytosis and Rac signaling. *Cell Res*. 2012;22:1479–1501.
54. Griffiths GS, Grundl M, Allen JS III, Matter ML. R-Ras interacts with filamin A to maintain endothelial barrier function. *J Cell Physiol*. 2011;226:2287–2296.

Investigative Ophthalmology & Visual Science